Chalcogenide Letters Vol. 21, No. 11, November 2024, p. 855 - 866

Improvement of porous silicon by adding CIGS NPs prepared by laser ablation method in water

H. R. Hassan, A. N. Abd*, M. J. M. Ali
Department of Physics, College of Science / Mustainsiriyah University, Iraq

Using a laser energy of no more than 600 mJ/pulse and a maximum of 500 pulses, this work selectively produced pure copper, indium, gallium, and selenide (CIGS) NPs using a laser ablation method with distilled water and n-type porous silicon prepared by the photoelectron etching method. The material exhibits quantum dot behavior, according to experimental investigations. Porous silicone bases were produced using a current density of 10 mA/cm^2 and an etching time of 15 min. Tests XRD, SEM, AFM, FTIR, UV, PL were conducted for the porous silicone and CIGS NPs to ensure that each of them is produced efficiently. To produce a hybrid junction\CIGS\Psi\n-Si\AG we see an enhancement of the spectral response of 0.71 A/W when a quantum dot is deposited on porous silicon.

(Received August 29, 2024; Accepted November 4, 2024)

Keywords: Porous silicon, AFM, UV, Laser ablation, CIGS, Photodetector

1. Introduction

Copper indium gallium selenide (CIGS) NPs show great promise for use in solar cell technology. In this work, a laser ablation technique was used to produce GS nanostructures [1]. A thin film is defined as an extremely thin layer of material, ranging in size from several micrometers to nanometers, applied to a given surface. Applications of thin films range widely, from electronic semiconductor devices to protection [2]. Due to their remarkable semiconductor properties, CIGS has emerged as one of the most promising absorbers for thin-film solar cells. In recent years, there have been several attempts to increase the production of these films. This paper discusses the challenges associated with scaling up current technology and the need for CIGS NPs in the photodetector industry [3]. Compared to previous methods, the procedure results in high material efficiency and provides good control over the morphological and structural properties of thin films [4]. The optical band gap of CIS is 1.02 eV [5], Achieving a higher conversion efficiency-based CIGS thin film will need getting closer to the ideal band gap of 1.5 eV for solar cell applications [6]. Silver was utilized to polarize nanoparticles put to the surface of porous silicon to produce a photodetector. CGISNPs were made specifically for this project to scatter the nanoparticles into the pores of porous silicon and boost the photodetector's spectrum responsiveness.

2. Experiment work

2.1. Preparing pours silicon by photoelectrochemical etching process

Starting substrates are n-type silicon crystalline wafers with "ρ =(2–20) Ω.cm, thickness of 508 μm, and orientation of (100)" . When photons with adequate energy reach the surface of an n-type silicon substrate, as seen in Figure 3, holes can be produced in the bulk. n-type substrate surface illumination using a 30 mW diode laser with a red wavelength of 650 nm. Using a current density of 10 mA/cm^2 to obtain an etched area of 0.785 cm^2.

* Corresponding author: ahmed_naji_abd@yahoo.com
https://doi.org/10.15251/CL.2024.2111.855

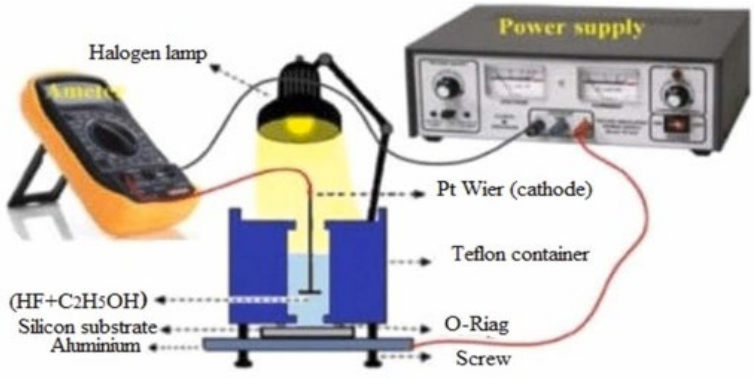

Fig. 1. The schematic diagram of PEC system.

2.2. Preparing (CIGS) NPs by laser ablation method

The first step preparation of CIGS pellet, by taking 8g of CIGS powder and grinding it with a pestle and CIGS powder pressing with 5 ton for 15 min by hydraulic press to obtain CIGS pellet with diameter 1.5 cm. The second phase involves, the target of CIGS was positioned at the bottom of a glass jar containing 10 mL of water only. The Nd: YAG laser (type HUAFEI), which operates at a wavelength of 1064 nm and 500 pulses with laser energy of (600) mJ per pulse, was used to execute the ablation procedure at normal atmospheric pressure. The three stages of the laser ablation process plasma formation, cavitation bubble growth, and bubble collapse with particle release are shown in Figures 2.

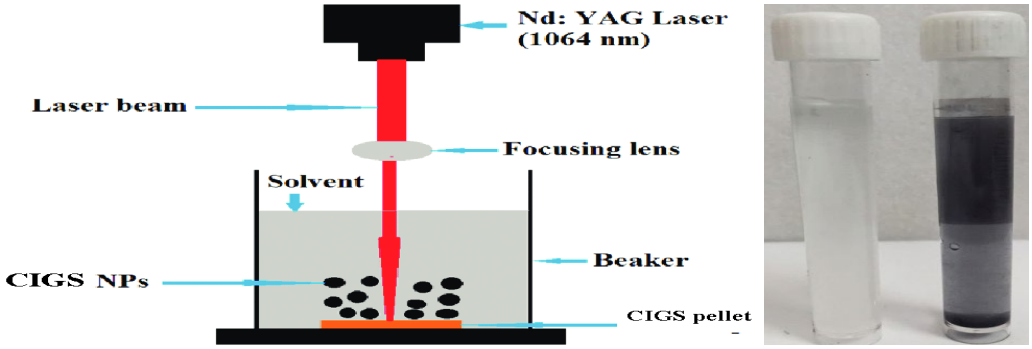

Fig. 2. Schematic diagram of P LAL method and Colloidal suspensions of CIGS NPs (left to right)

2.3. Thin film deposition

A CGIS film has been deposited on glass, quartz, and PSi samples using the drop casting technique (see figure 3). This technique yields the most production from a basic equipment and negates material waste when used to manufacture a wide range of thin films.

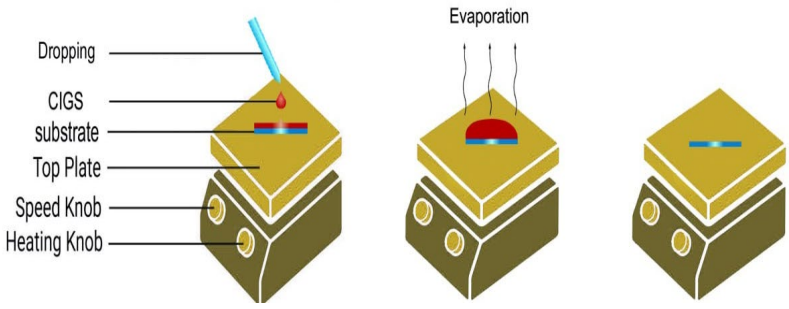

Fig. 3. Schematic diagram drop casting method experimental set up.

3. Results and discussion of n-porous silicon

X-ray diffraction (XRD) of the n-PSi material is displayed in Figure (4). Additionally, the image displays a single peak at 2θ = 69.74° that is only oriented along the (400) direction, confirming the PSi layer's mono-crystalline structure and its membership in the (400) reflecting plane of Si in a cubic structure (as per ICDD N 1997 and 2011 JCPDS) [7]. Using the Debye-Scherer formula [8], the samples' crystallite size (D) was determined and listed in Table 1.

$$\boldsymbol{D} = \mathbf{0.9}\,\boldsymbol{\lambda} / \text{FWHM}\,\boldsymbol{\cos\theta} \quad (1)$$

where FWHM is the Full Width at Half Maximum and θ =34.87^{O}, The density of dislocations is calculated using a relation:

$$\sigma = 1/D^2 \quad (2)$$

To find out and calculate the inter layer distance (d) between the parallel crystal planes in the lattice from the following equation:

$$n\lambda = 2d\sin\theta \quad (3)$$

where d is the distance between diffracting planes, and n=1

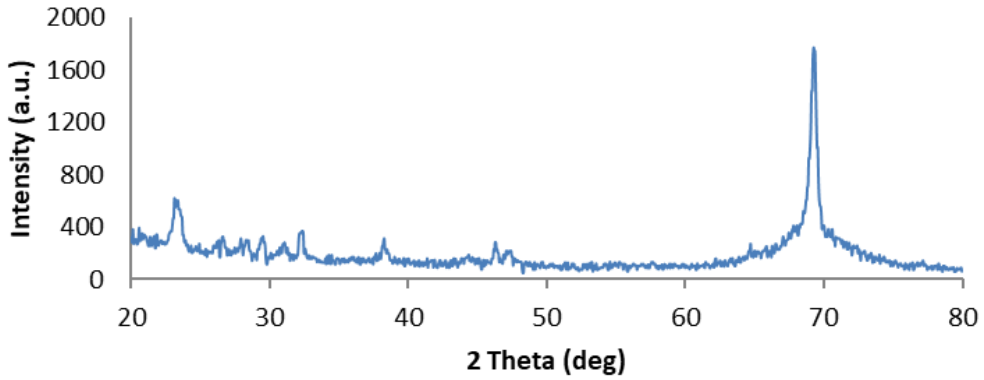

Fig. 4. XRD spectra of n-Psi.

Table 1. Parameters of porous silicon.

Etching time (min)	2Θ (deg)	d(A)	FWHM (deg)	D (nm)	Lattice constant (nm)	Strain x10^{-4}
10	69.74	1.357	0.14	71.16	1.358	29.05

This section includes AFM pictures that examine the structural characteristics and porosity of PSi. Granularity accumulation distribution charts and three-dimensional pictures of the anodized (n) PSi at the same etching time and current density are displayed in Figure (5). Using software for AFM analysis, the average grain size for n-Si is determined fig. 5). The AFM investigations of the n-PSi layer reveal smooth and uniform structures on its surface, distributed uniformly on the surface. with a matrix of randomly oriented Nano-crystalline silicon pillars pointing in the same direction making up the film. The characteristics of the porous silicon surface are shown in Table (2) [9].

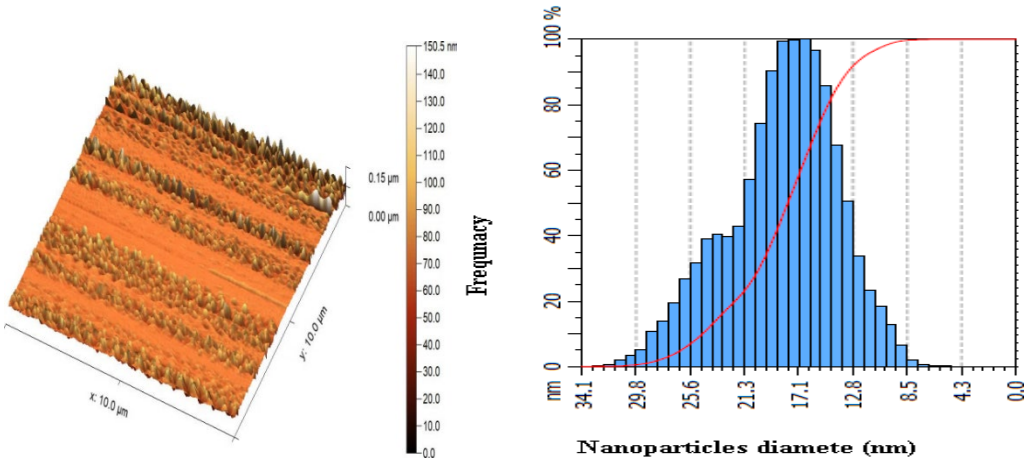

Fig. 5. AFM 3D-images with chart distribution of the porous silicon (n-PSi)

Table 2. The parameter of porous silicon.

Sample	Average diameter (nm)	Root main square (nm)	Roughness average (nm)
PSi	73.098 nm	9.754 nm	6.349 nm

The FTIR spectra of n-PSi produced are displayed in Figure (6). Due to its high surface area and infrared transparency, silicon is a useful material for Fourier transforms infrared spectra (FTIR) analysis, a robust and easy-to-use technique for identifying the chemical bonds of porous silicon surfaces. The huge surface area of porous silicon enables the high surface sensitivity of the adsorbed molecules. Note that occasionally the surface could unintentionally oxidize. There are many distinct peaks with different intensities. The peaks at (3777.18, 3342.29, 2919.18, 2097.73, 1641.64, 1442.37, 1032.51 and 636.82) cm-1 suggest the manufacture of porous silicon. The little peak at 636 cm-1 is associated with the [C-H] Waggener mode, whereas bond 1032 is associated with [Si-O-Si]. Peaks at 1442.3 and 1641.64 cm^{-1} show that the [C-O] is extending. Because carbon and silicon are located in the same periodic table column, carbon can readily take the place of a silicon atom, resulting in the presence of carbon in the porous structure. A prominent wide band is noted at around 2097 cm-1 as a result of [C=C] Waggener. Furthermore, the last bonds for ethanol, 3342 and 3777 cm-1, indicated to the O-H [10]. During anodization in air, new chemical bonds are formed due to different [Si-H] and [Si-O] chemical bond configurations seen in the IR spectra. These new chemical bonds appear as a broad transmission band on the surface. It should be highlighted that there wouldn't be an infrared peak in the spectra if a molecule had such great symmetry that stretching a bond wouldn't alter the dipole moment [11–12].

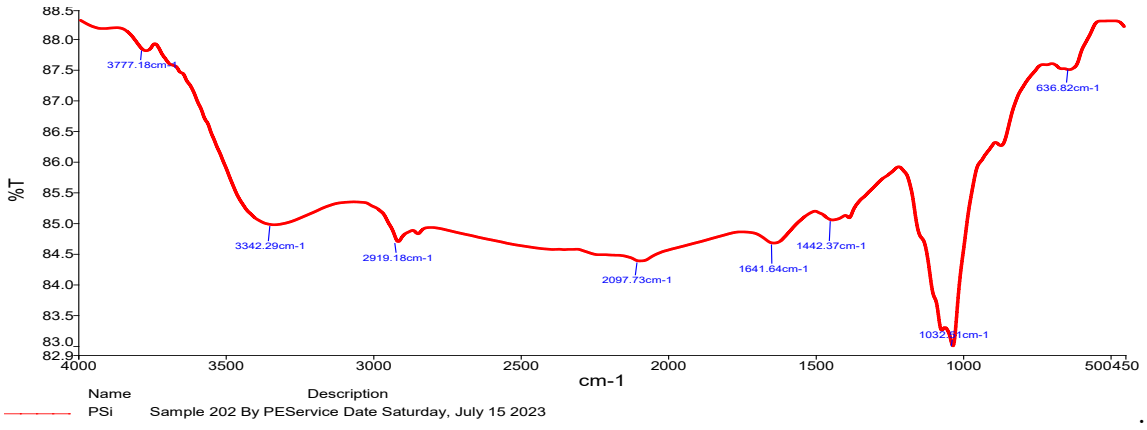

Fig. 4. FT-IR spectrum of synthesized n-PSi

The PL spectra of n-type PSi, produced at current densities of 10 mA/cm^2 and etching times of 15 minutes, are displayed in Figure (7). The measurement range for PL spectra was (600-100) nm. The emission peak of silicon and n-type PSi at 700 nm is depicted in figure 7. According to reference [13], the results show that there is a noticeable amount of luminescence confined to the constrained silicon structures in the spectral bands of 1.78 eV and 1.24 eV. This could be because of photoluminescence from the confined silicon structures.

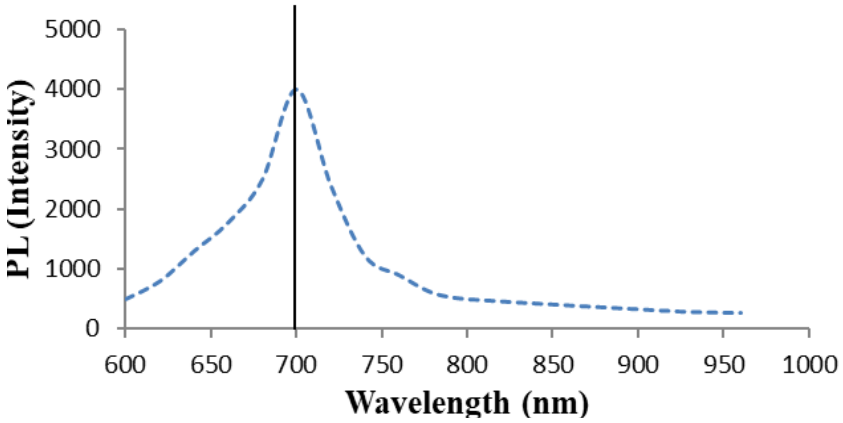

Fig. 7. Photoluminescence spectra of n-Psi.

4. Results and discussion of CIGS nanoparticle

Figure (8) shows of a diffraction peak at roughly 26.38 matches to a cubic phase structure's (100) plane. A prominent orientation along the (100) direction is constantly seen in the X-ray diffraction (XRD) patterns; this orientation is suggestive of the Carbon blende crystal structure. The results obtained were compared with the JCPDS values for CIGS (Data file: 75-2086-cubic) [14]. When it comes to peak breadth, the circumstances are the opposite. Increased 6 atomic mobility leads to the formation of larger-dimensional crystallites, which explains the observed phenomenon. The parameters that were determined using X-ray diffraction (XRD) tests are shown in Table (3). The Debye-Scherer formula's first equation was utilized to calculate the samples' crystallite sizes (D).

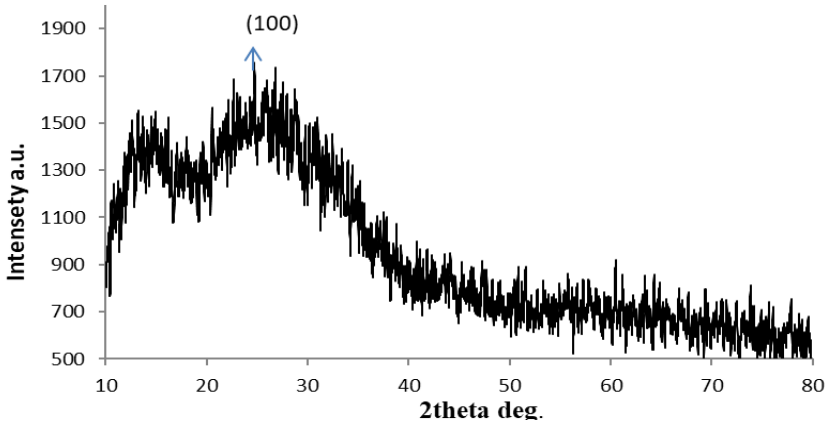

Fig. 8. XRD of CIGS thin film.

Table 3. XRD data of CIGS NPS.

2 Theta (deg)	FWHM (deg)	hkl plane	D nm
26.38	0.208	100	40.38

SEM pictures of CIGS NPs generated by laser ablation technique and placed on glass substrate are presented in Figure (10). SEM images verify the unique morphology of these NPS. These nanoparticles (NPs) exhibit an irregular morphology and consist of many irregular particles with an average size ranging from 35 to 60 nm. The calcination impact and the product's SEM data are shown in Fig. (9).Using SEM examination, the surface morphology of the generated CiGs nano-structure was examined. CiGs has a mean particle diameter of 818.21 nm, a spherical shape, and high homogeneity. However, a few particles were also discernible.

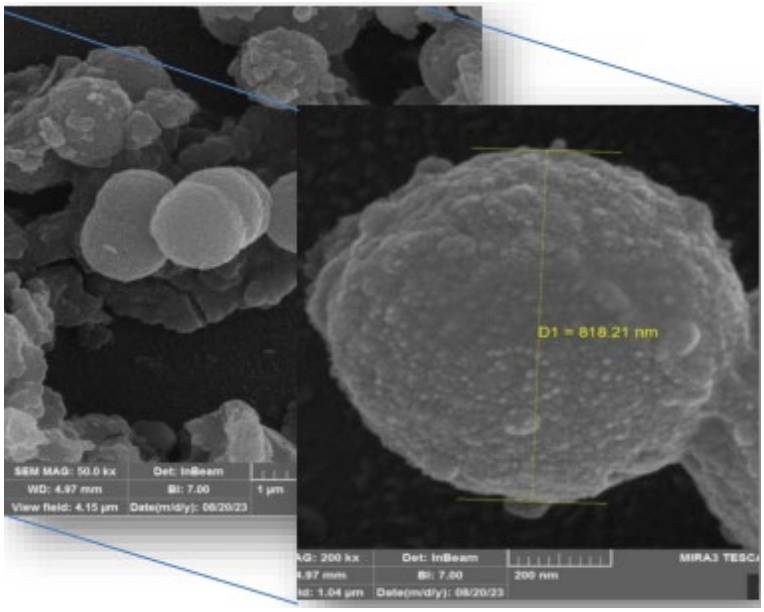

Fig. 9. SEM images of CIGS Thin film deposited at a room temperature and prepared by laser ablation.

Figure (10) displays the granularity accumulation distribution chart and 3D AFM pictures of CIGS NPs manufactured using the laser ablation method. The CIGS NPs are vertically aligned. The figure(10) shows a number of small peaks facing upward and aligned horizontally, forming the nanoscopic surface. The distribution of these particles is orderly, while sometimes a difference appears in the shape and distribution of the particles, especially at the edges, because they contain sharp peaks. Uniform grain composition with good dispensability. The CIGS NPs generated by laser ablation agglomerated to form average particles (10.7874 nm), and the estimated values of the root mean square RMS of the average grain size and surface roughness were computed using specialized software. The results are reported in Table (4). Given that the average grain size measurements agree with the XRD estimates, it is clear that the surface is homogeneous. Grain size and the root mean square of surface roughness both rise with laser energy. Three-dimensional images show that individual columnar grains extend vertically, and that the grains are uniformly distributed throughout the scanning zone. For photodetectors, this surface characteristic is essential (PDs).

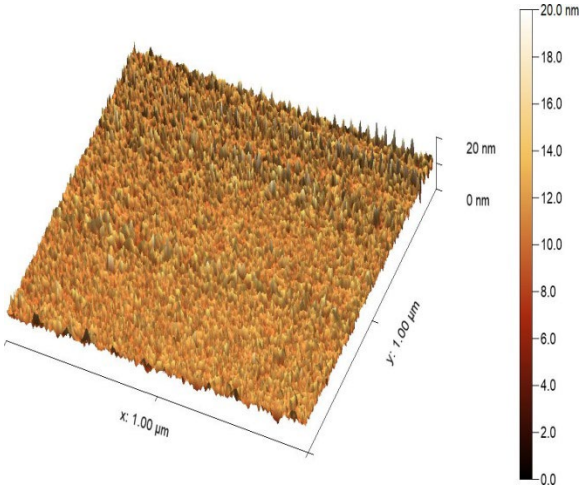

Fig. 10. 3DAFM image of CiGs nano-structure.

Table 4. Parameters of CiGs nano-structure.

Nanoparticle	*Average Grain size (nm)*	*Roughness average (nm)*	*Root mean square (nm)*
CGTS	10.7874	1.1947	1.5146

FTIR of CIGS produced by laser ablation method are displayed in Figure (11). Due to its high surface area and infrared transparency, (FTIR) analysis, a robust and easy-to-use technique for identifying the chemical bonds of CIGS surfaces. It should be noted that the surface may inadvertently oxidize from time to time. There are numerous unique peaks of varying strengths. The manufacturing of CIGS is indicated by the peaks at (737,1650,2123,3480) cm-1 as shown in table (6) The [C-H] Waggener mode can be linked to the little peak at 737 cm-1, but the bond. Peaks located at 1650 cm-1 indicate a stretching of the [C-O]. Additionally, the peak2123 located at[C=C], the last bond 3480 cm-1, indicated to the O-H [15].

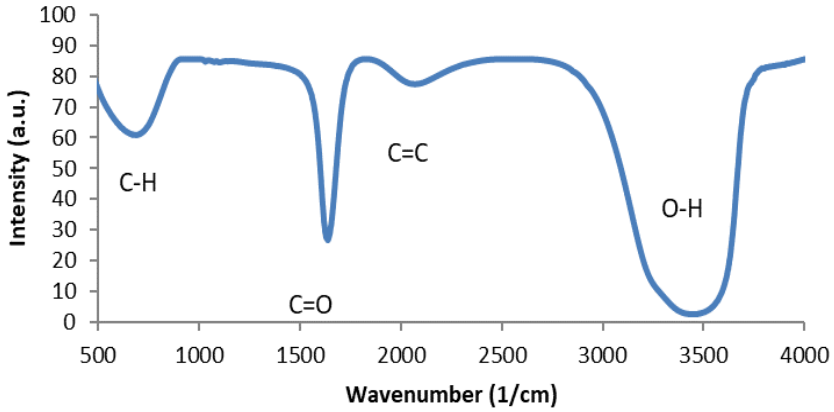

Fig. 11. FTIR spectra of CIGS NPS samples.

The absorption spectra of CIGS NPs made using the laser ablation approach are displayed in Figure (12). One helpful tool for analyzing nanomaterials is the absorption properties. It is evident that below 200 nm, the absorption is drastically reducing. Due to the quantum size effect; it is observed that there are notable fluctuations in absorption spectra in the 200–300 nm range. This phenomenon can be attributed to the creation of CIGS NPs. This outcome closely aligns with references [19, 20].

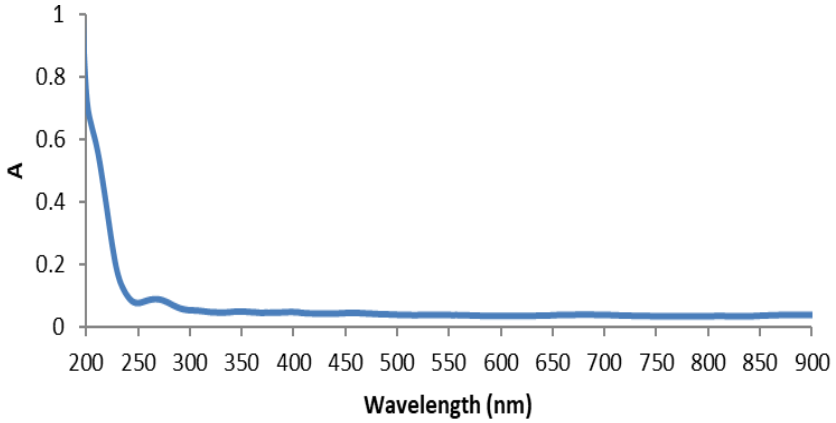

Fig. 12. Optical absorption for CIGS.

By projecting the linear portion of the (αhν)2 against hν figure to the photon energy axis, the band gap of CIGS NPs may be calculated [18]. A "blue shift" of 0.8 eV from the typical bulk band gap (Eg=1.7 eV) is indicated by the solution containing CIGS NPs, which has a direct band gap of 2.5 eV for CIGS NPs (see Figure (13). There could be a nanoscale influence causing the blue shift.

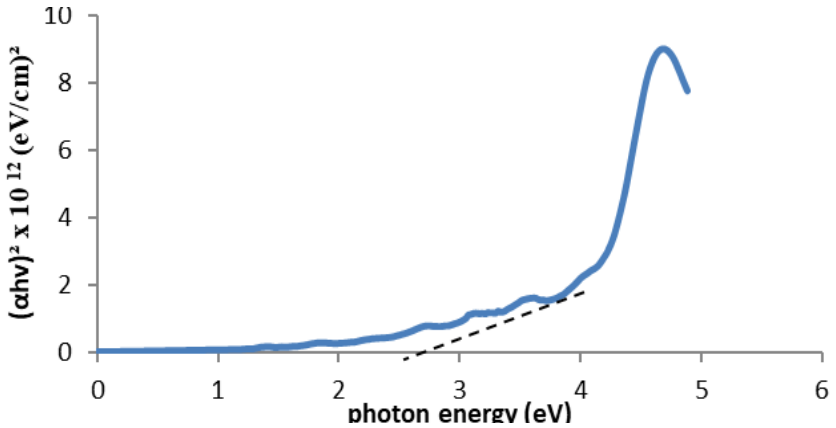

Fig. 12. $(\alpha h\nu)^2$ versus photon energy gap of CIGS.

5. Fabrication of AG/CIGS QD /PSi/c-Si/AG photodetactor

After preparing the PSi, drying it with the heat of a tungsten lamp, and preparing CIGSNPs, the back side of the PSi was coated in the shape of a circle with a diameter of 2 mm, then five drops of CIGS NPs were added, then coated with silver adhesive with a diameter similar to the back diameter, as shown in the Figure (14).

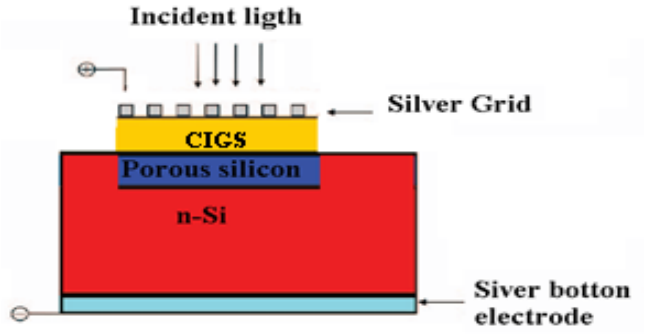

Fig. 14. Fabrication of Ag/ CIGS /PSi/Si/Ag heterojunction

6. Photodetector characterization

The investigation of spectral responsively in structures is conducted within the wavelength range of (350–900) nm, utilizing a 5V bias. The calculation of spectral responsivity is performed using the equation (4) [21].

$$R_\lambda = \frac{I_{Ph}}{P} \quad \left(\frac{A}{W}\right) \tag{4}$$

where Iph represents the photocurrent, while P denotes the input power. The structure referred to as Ag/CIGS/PSi/c-Si/Ag comprises of two hetero-junctions. in Figure 15. The curve's spectral responsivity is composed of a single peak (Three peaks connected together) make-up of the the absorption edge of CIGS NPs at 550 nm, and the second area can be attributed to the absorption edge of PSi occurring at a wavelength of 750 nm. Also, the last peak for n-silicon at 800 nm).

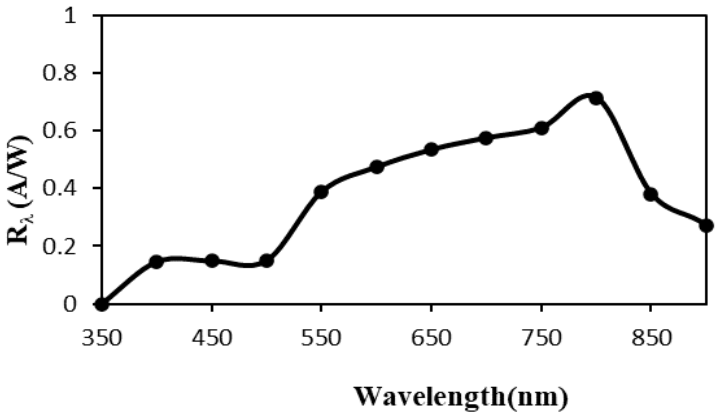

Fig. 15. Responsivity of CIGS/PSi/n-Si photodetectors.

A measure of quantum efficiency is the ratio of electrons produced to photons incident. When light contacts the photo emissive detector, which is what it is called, free electrons are released from its surface. Should the detector be a p-n junction semiconductor device. The term "quantum efficiency" refers to a different method of quantifying how well incident optical energy can be used to produce an electrical current output. The quantum efficiency Q, expressed as a percentage, can be connected to the responsiveness using the following equation:

$$Q = R_\lambda \frac{1.24}{\lambda_{(\mu m)}} \; X\,100\% \tag{5}$$

R (λ): is the responsively (in amperes per watt) of the detector at wavelength λ nm [22].

Figure (16) shows the Ag/CIGS/PSi/c-Si/Ag quantum efficiency curve. higher light absorption, higher diffusion length and depletion width, decreased surface defect states, and increased carrier collection efficiency cause the spectral responsivity curve to reach its maximum value (100%) at 800 nm.

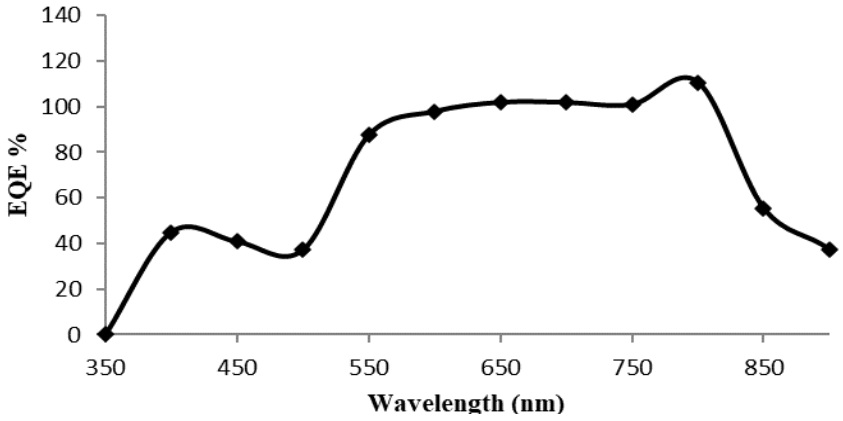

Fig. 15. Quantum efficiency as a function of wavelength of CIGS/PSi/n-Si photodetectors.

7. Conclusion

In conclusion, it is clear that the previously presented arguments are in favor of the idea that the subject at hand merits more research and examination. CIGS and PSi materials were used to successfully manufacture a nano-structure hetero-junction photodetector using the pulsed laser

ablation in water (PLAL) technology and photo electrochemical etching, respectively. The colloidal suspension was deposited on PSi substrate to fabricate the AG/CIGS/PSi/n–Si/AG photodetector which exhibits improved properties of PSi., then the spectral responsivity approximately 0.65 A/W at wavelenghth(800)nm. This enhancement can be attributed to the following elements:

1. One potential area of improvement is the enhancement of light absorption.
2. One approach to enhance the performance of a semiconductor device is to increase the depletion width and diffusion length.
3. The surface defect states were minimized.
4. One potential approach to enhance the carrier collection efficiency is through an increase in its value.
5. One approach to mitigating the dark current is through reduction.

References

[1] Mousavi, S. H., Müller, T. S., Karos, R., De Oliveira, P. W. Journal of Alloys and Compounds, 659, 178-183, 2016; https://doi.org/10.1016/j.jallcom.2015.10.261

[2] Mohan, R., Paulose, R. Photoenergy and thin film materials, 157-192.2006.

[3] Renganathan, N. G., Subramanian, M. V., Mohan, S., International Journal of Engineering, Science and Technology, 3,1, 2009.

[4] Venkatachalam, M., Kannan, M. D., Jayakumar, S., Balasundaraprabhu, R., Muthukumarasamy, N. (2008). Thin Solid Films, 516(20), 6848-6852, 2008; https://doi.org/10.1016/j.tsf.2007.12.127

[5] Venkatachalam, M., Kannan, M. D., Jayakumar, S., Balasundaraprabhu, R., Muthukumarasamy, N. Thin Solid Films, 516(20), 6848-6852, 2008; https://doi.org/10.1016/j.tsf.2007.12.127

[6]. Ravi Dhas, C., Christy, A. J., Venkatesh, R., Kirubakaran, D. D., Sivakumar, R., Ravichandran, K., Sanjeeviraja, C. , Materials Research Innovations, 21(5), 286-293,2017; https://doi.org/10.1080/14328917.2016.1214226

[7] JCPDS -International centre for diffraction data, USA card No.77-2307

[8] H. Hernandez-Contreras, C. Mejia-Garcia, G. Contreras-Puente, Thin Solid Films 451-452, 203, 2003; https://doi.org/10.1016/j.tsf.2003.10.157

[9] H. Hernandez-Contreras, C. Mejia-Garcia, G. Contreras-Puente, Thin Solid Films 451-452, 203, 2004; https://doi.org/10.1016/j.tsf.2003.10.157

[10] Amarie S, Ganz T, Keilmann F (November 2009), Optics Express 17 (24): 21794-801, 2009; https://doi.org/10.1364/OE.17.021794

[11] S.M. Sze and K. Kowk, Pysical of Semiconductor Devices, John Wiley and Sons ,2nd Ed 1981.

[12] S.M. Sze, K.Kowk ,Physical of Semiconductor Devices, John Wiley and Sons ,3rd Ed.,2007.

[13] F.Dughiero, A.Candeo, E.Sieni; Dipartimento di Ingegneria Elettrica, Universit di Padova;

[14] JCPDS -International centre for diffraction data, USA card No.77-230

[15] JCPDS -International centre for diffraction data, USA card No.77-2307

[16] Sang-Hyun Choi, Hongju Songb, Kyu Park, Jun-Ho Yumb, Seok- Soon Kimb, Journal of Photochemistry and Photobiology A: Chemistry 179, 135-141.2006.

[17] N. F. Habubi, R. A. Ismail, A. N. Abd and W. K. Hamaoudi, Indian J. Pure Appl. Phys. 53 718. 2015.

[18] JCPDS -International centre for diffraction data, USA card No.77-2307

[19] S.M. Sze and K.Kowk ,"Physical of Semiconductor Devices", John Wiley and Sons, 3rd Ed.,2007

[20] Mustafa Younis Ali1, Wedian K. Abad, Harakat Mohsin Roomy and Ahmed N. Abd, NanoWorld Journal NanoWorld Journal 9, 89-93 ,2023.

[21] Bahaa J. Alwan; Ahmed N. Abd; Neihaya H. Zaki, AIP Conf. Proc. 2834, 090012, 2023; https://doi.org/10.1063/5.0176321

[22] A. N. Abd, Improved photoresponse of porous silicon photodetectors by embedding CdS NPs World ScientiIc News 19, 32, 2015.